

DFT Investigation, Chemical Reactivity Identification and Molecular Docking of 2(E)-1-(3-bromothiophene-2-yl)-3-(furan-2-yl)prop-2-en-1-one

A. Nataraj^{1*}, K. Anitha¹, B. Narayan²

¹Department of Physics, University of Sri Ramaswamy Memorial, Tamilnadu, India

²Department of Chemistry, University of Mangalore, Karnataka, India

Research Article

Received: 02-Feb-2022,
Manuscript No. JPAP-22-
55273; **Editor assigned:** 04-
Feb-2022, Pre QC No. JPAP-22-
55273 (PQ); **Reviewed:** 18-Feb-
2022, QC No. JPAP-22-55273;
Revised: 04-Apr-2022,
Manuscript No. JPAP-22-55273
(R); **Published:** 14-Apr-2022,
DOI: 10.4172/2320-
2459.10.4.006.

***For Correspondence:** A. Nataraja
Department of Physics, University
of Sri Ramaswamy Memorial,
Tamilnadu, India

E-mail: sakuraj86@yahoo.co.in

Keywords: FT-IR; FT-Raman; UV-
Vis absorption; Antifungal activity;
Anti-inflammatory potential;
Molecular docking

ABSTRACT

Chalcone derivative of 2(E)-1-(3-Bromothiophene-2-yl)-3-(furan-2-yl)prop-2-en-1-one (BTF) molecule was probed by quantum chemistry method with the Gaussian 09W software package. The infrared and Raman spectra were computed by DFT method under the B3LYP level of theory and the Potential Energy Distribution (PED) was predicted for detailed vibrational assignments. The electronic properties were analyzed using UV-Vis absorption spectra within the range of 200-600 nm. In addition, EHOMO energy (-6.367 eV), ELUMO energy (-2.705 eV), the energy difference (3.662 eV), softness (0.546 eV) and electrophilicity index (5.618 eV) were determined to understand the reactivity, stability and biological potency of the BTF molecule. Molecular Electrostatic Potential (MEP) was accounted for the identification of reactive sites. The intra molecular interactions and charge delocalization of the compound were examined using Natural Bond Orbital (NBO) analysis. Non-linear optical features were demonstrated from the first order hyperpolarizability. Based on the above results the BTF compound was investigated for further biological investigation. The BTF compound was screened for their in vitro antifungal activity in Sabouraud Dextrose Agar Medium (SDA) and which shows moderate antifungal activity. *In vitro* Anti-inflammatory activity was evaluated using Bovine Serum Albumin (BSA) protein denaturation assay at different concentrations. A molecular docking was performed to investigate the interactions between ligand (BTF) and the Arachidonate 5-lipoxygenase (ALOX-5) protein.

INTRODUCTION

Thiophene and its derivatives are interesting due to their biological activities and pharmacological applications. Chalcone compounds have been largely investigated for their chemical flexibility and potential applications as NLO media and different

types of synthetic materials and stabilities [1-3]. Chalcone compounds enhance the Second Harmonic Generation (SHG) because of their strongest inter molecular interactions and delocalization of 'π' electron conjugation in the molecular system [4]. In recent years, chalcone and its derivatives are of great interest since they exhibit a large number of medicinal and pharmacological activities such as antibacterial, anticancer, antituberculosis, anti-inflammatory, antifungal, antiviral, antimicrobial, antimalarial, antitumor, analgesic and antidepressant [5,6]. For this reason, theoretical and experimental analysis of BTF is significant. In this present article, the structural characterization of BTF has been extensively studied in this article. It was experimentally investigated using the techniques of FT-IR and FT-Raman. Molecular electronic transactions (UV-Vis) were deliberated through TD-DFT method. The chemical reactivity of the given molecule is examined using molecular reactivity descriptors such as HOMO-LUMO, NBO and MEP maps using the DFT method. Molecular docking was used to simulate the interactions of the title compound with the Arachidonate 5-lipoxygenase (ALOX-5) protein at the active site.

MATERIALS AND METHODS

Spectral measurement

The FT-IR spectrum of the BTF molecule was investigated in KBr beam splitter with a Perkin Elmer spectrum of resolution ± 1 cm^{-1} of spectrometer in the scale range 500-4000 cm^{-1} . FT-Raman Bruker RFS 27 spectrometer were used to record the FT-Raman spectrum within the region 500-4000 cm^{-1} and equipped with Nd: YAG laser source operating at 1064 nm. The spectral resolution is ± 2 cm^{-1} . The UV-Vis absorption spectrum of the title compound was measured by methanol solvent and a resolution of 0.05 nm in the wavelength range of 200-600 nm.

Agar disc diffusion method

The agar diffusion technique was followed for the antifungal susceptibility test. The Petri plates were prepared by pouring 10 mL of Sabouraud Dextrose Agar and were allowed to solidify. Plates were dried and 0.1 mL of standardized inoculum suspension was added and uniformly spread. The excess inoculum was drained and left to dry for five minutes. The discs were then applied to incubate with *Aspergillus niger*, *Trichophyton* and *Microsporum gypseum* BOD incubators at 28°C for 72-96 hrs. Then inhibition zone was evaluated from the edge of the disc to the inner margin of the surrounding pathogens. Each assay in this experiment was repeated thrice.

Anti-inflammatory activity

The protein denaturing test was carried out in accordance with the procedure described by Mizushima and Sakat et al. The 500 μL volume of 1% bovine serum albumin were added to 100 μL of test dilution. The mixture was kept at room temperature for 10 min, and then heated for 15-20 min at 51°C. Then the solution was brought to normal room temperature and absorbance at 660 nm was recorded. Acetylsalicylic acid was used as standard. The process was performed in triplicates and protein denaturation inhibition percentage was calculated using the formula:

$$\% \text{ Inhibition} = 100 - [(A1 - A2) / A0] \times 100$$

Where, A1 is sample absorbance, A2 is product control absorbance and A0 is the absorbance of the positive control.

Computational details

The optimized geometric parameters of bond lengths, bond angles and dihedral angles and vibrational wavenumbers were computed by a B3LYP function of 6-311+G (d,p) basis set. Using the same level of theory, Natural Bond Orbital (NBO) method was explored through calculating first order hyper polarizability to understand the various interactions between donor orbitals and the acceptor orbitals of different subsystems. The charge transfer properties are examined using HOMO and LUMO analysis [7]. The biological activity of the molecule was investigated by auto dock software [8] by using Auto dock tools 4.2.1

and PyMOL is used to shows the interaction between protein and ligand.

RESULTS AND DISCUSSION

Molecular geometric parameters of BTF

The optimized structural parameters for the BTF molecule are listed in Table 1.

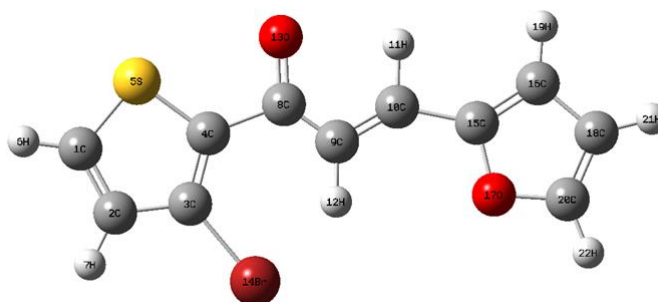
Table 1. The geometrical parameters (Bond lengths (Å) and Bond angles (degree)) of BTF calculated at DFT/B3LYP.

Parameters	Bond lengths (Å)		Parameters	Bond angles (deg)	
	Experimental values	Theoretical values		Experimental values	Theoretical values
C1-C2	1.369	1.366	C2-C1-S5	113	112.5
C1-S5	1.727	1.719	C2-C1-H6	127.6	127.3
C2-C3	1.415	1.42	S5-C1-H6	119.9	120
C3-C4	1.397	1.382	C1-C2-C3	113	111.7
C3-Br14	1.907	1.907	C2-C3-C4	114.8	114.4
C4-S5	1.727	1.754	C2-C3-Br14	118.9	118.3
C4-C8	1.481	1.485	C4-C3-Br14	127.6	127.3
C8-C9	1.466	1.472	C3-C4-S5	108.3	109.2
C8-O13	1.221	1.229	C3-C4-C8	127.6	136.5
C9-C10	1.33	1.35	S5-C4-C8	116.1	114.1
C10-C15	1.423	1.429	C1-S5-C4	92.6	91.97
C15-C16	1.346	1.374	C4-C8-C9	119.4	120.1
C15-O17	1.367	1.373	C4-C8-O13	119.7	117.9
C16-C18	1.407	1.424	C9-C8-O13	120.7	121.8
O17-C20	1.362	1.355	C8-C9-C10	121.1	119.6
C18-C20	1.327	1.363	C9-C10-C15	127.3	126.1
C1-H6	0.95	1.079	C10-C15-C16	131.8	131.5
C2-H7	0.95	1.08	C10-C15-O17	118.7	119.4
C9-H12	0.95	1.079	C16-C15-O17	109.3	109
C10-H11	0.95	1.085	C15-C16-C18	107.3	106.8
C16-H19	0.95	1.078	C15-O17-	105.9	107.3

			C20		
C18-H21	0.95	1.078	C16-C18-C20	106.2	105.9
C20-H22	0.95	1.077	O17-C20-C18	111.1	110.7
-	-	-	O17-C20-H22	124.4	115.9
-	-	-	C18-C20-H22	124.4	115.9
-	-	-	C1-C2-H7	124.9	124.7
-	-	-	C3-C2-H7	123.1	123.4
-	-	-	C8-C9-H12	119.4	119.7
-	-	-	C10-C9-H12	119.4	120.6
-	-	-	C9-C10-H11	116.3	118.1
-	-	-	C15-C10-H11	116.3	115.6
-	-	-	C15-C16-H19	126.3	125.5
-	-	-	C18-C16-H19	126.3	127.5
-	-	-	C16-C18-H21	126.9	127.6
-	-	-	C20-C18-H21	126.9	126.3

The numbering scheme of the atoms of the BTF molecule gained from an optimized structure is manifest in Figure 1.

Figure 1. Structure and atoms numbering of 2(E)-1-(3-bromothiophen-2-yl)-3-(furan-2-yl)prop-2-en-1-one optimized with B3LYP/6-311+G(d,p) approach.



The geometric structure was fully optimized in the higher level of theory (DFT/B3LYP) as well as the basis set. The stability of the optimized geometry was confirmed owing to the lack of negative wave numbers [9]. The optimized geometrical parameters were compared with structurally similar molecules available in literature, i.e 2(E)-1-(3-bromo-2-thienyl)-3-(4-chlorophenyl)-prop-2-en-1-one and (E)-3-(furan-2-yl)-1-phenylprop-2-en-1-one [10,11]. For the BTF compound C–C bond lengths were C1–C2= 1.366/1.369 Å (DFT/XRD), C2–C3=1.420/1.415 Å, C3–C4=1.382/1.397 Å, C4–C8=1.485/1.481 Å, C8–C9=1.472/1.466 Å, C9–C10=1.350/1.330 Å, C10–C15=1.429/1.423 Å, C15–C16=1.374/1.346 Å, C16–C18=1.424/1.407 Å and C18–C20= 1.363/1.327 Å. There are significant similarities between experimental and theoretical data. The C3–Br14 bond in non-polar bond as a consequence of mostly equal sharing of electrons because of electronegativity difference (ΔEN) and higher bond length 1.907/1.907 Å is exactly matched with the experimental value. The C-S bond lengths give a higher value as the lone pair of electrons on S atom repel with the electron on the C atom in the ring. The bond length of C4–S5 and C1–S5 having 1.719/1.727 Å and 1.754/1.727 Å and the calculated value is almost equal to the observed bond length. The C9=C10 bond length is compared to the other nonpolar C=C bond length where the value is less due to the adjacent (C8–O13) carbonyl group which undergoes ketoenol tautomerism and gives rise to the chemical equilibrium. In present work, the C–H bond lengths are normally large for DFT/B3LYP theoretical calculations. For the BTF molecule, at C3 position of the thiophene ring, the bond (DFT/EXP) angles C2–C3–C4=114.4°/114.8°, C2–C3–Br14=118.3°/118.9° and C4–C3–Br14=127.3°/127.6° are in line with the literature data. Similarly, at C15 position of furan ring, the bond angles C10–C15–C16=131.5°/131.8°, C10–C15–O17=119.4°/118.7° and C16–C15–O17=109.0°/109.3° and these values were indicate that there is an interaction between C=C and neighboring atoms. C4–C8–C9=120.1°/119.4°, C4–C8–O13=117.9°/119.7° and C9–C8–O13=121.8°/120.7° these deviation angle shows the hyper conjugative interaction between C=O and thiophene ring. The difference between theoretical and experimental geometry be attributed to the fact that calculations were performed on isolated molecule in the gaseous phase to predict theoretical results and the solid state for experimental results.

Vibrational spectral analysis of BTF

The observed (FTIR and FT-Raman) and computed vibrational frequencies along with their absolute intensities and Potential Energy Distribution (PES) with suitable assignments are given in Table 2.

Table 2. The experimental and theoretical vibrational spectra and proposed assignments of BTF molecule at B3LYP method with 6-311+G (d,p) basis set.

Mode	Experimental		Theoretical		Reduced mass (amu)	Force constant (mdyne/Å)	Vibrational assignments
	wavenumbers		Wavenumbers				
	(cm ⁻¹)		(cm ⁻¹)				
	FT-IR	FT-Raman	Un scaled	scaled			
1	3096	3047	3276	3181	1.105	6.995	$\nu_{CH}(98)$
2	-	-	3254	3160	1.096	6.846	$\nu_{CH}(100)$
3	-	-	3244	3150	1.092	6.771	$\nu_{CH}(95)$
4	-	-	3240	3147	1.099	6.804	$\nu_{CH}(99)$
5	-	-	3231	3138	1.089	6.705	$\nu_{CH}(99)$

6	-	-	3218	3125	1.089	6.65	vCH(100)
7	-	-	3171	3079	1.089	6.452	vCH(99)
8	1641	1640	1693	1644	6.878	11.62	vOC(38)+vCC(38)
9	1585	1581	1626	1579	8.939	13.92	vOC(49)+vCC(14)
10	1550	1548	1584	1568	5.072	7.504	vCC(62)+βHCC(10)
11	-	-	1530	1514	6.408	8.838	vCC(74)
12	1487	1476	1503	1487	4.675	6.225	vCC(54)+βHCO(17)
13	-	-	1440	1425	7.744	9.47	vCC(75)
14	140 1	1396	1421	140 6	2.802	3.334	vCC(31)+βHCC(19)+βHCO(12)+ vOC(10)
15	-	-	1376	1362	2.324	2.593	βHCC(60)+vCC(17)
16	1316	-	1344	1330	1.836	1.956	βHCC(47)+vCC(13)
17	-	1285	1308	1294	2.042	2.061	βHCC(48)+vCC(12)
18	1268	-	1284	1271	2.557	2.485	vCC(35)+βHCC(20)+βCCO(10)
19	1218	-	1232	1219	2.024	1.81	βHCC(23)+βHCO(14)+ vCC(11)
20	1182	-	1198	1185	2.085	1.765	βHCC(35)+vCC(18)
21	-	-	1176	1164	2.073	1.692	vOC(41)+βHCO(30)+vCC(13)
22	-	-	1172	1160	2.181	1.767	vCC(46)+βHCC(29)
23	-	-	1112	1100	1.323	0.964	βHCC(62)+vCC(14)
24	1084	-	1106	1094	2.215	1.597	vOC(32)+vCC(14)+βHCC(12)
25	1022	1019	1040	1029	1.31	0.835	βHCC(66)+vCC(23)
26	-	-	1010	999	1.142	0.687	τHCCC(93)

27	975	976	987	977	4.575	2.631	$\nu_{CC}(42)+\nu_{SC}(12)$
28	926	-	943	933	3.74	1.961	$\nu_{OC}(51)\nu+\beta_{CCO}(11)+\nu_{CC}(10)$
29	882	-	902	892	6.147	2.949	$\beta_{COC}(75)+\nu_{OC}(15)$
30	-	-	898	888	1.623	0.772	$\tau_{HCCH}(42)+\tau_{HCCC}(36)$
31	-	-	895	885	1.31	0.619	$\tau_{HCCH}(71)+\delta_{CCCH}(19)$
32	-	-	890	881	1.59	0.743	$\tau_{HCCH}(32)+\tau_{HCCC}(31)+\delta_{CCOH}(13)$
33	-	860	881	872	4.633	2.119	$\beta_{CCC}(73)$
34	-	-	850	841	5.604	2.386	$\beta_{CCO}(31)+\nu_{SC}(16)+\beta_{CCC}(14)$
35	820	-	832	823	1.402	0.572	$\delta_{CCCH}(62)+\delta_{CCOH}(19)$
36	-	-	809	800	6.632	2.562	$\beta_{CCC}(29)+\nu_{SC}(25)$
37	-	-	760	752	1.272	0.434	$\delta_{CCOH}(55)+\delta_{CCCH}(22)+\tau_{HCCH}(15)$
38	745	-	751	743	2.57	0.854	$\delta_{OCCC}(34)+\delta_{CCCH}(26)$
39	701	-	728	720	1.737	0.544	$\delta_{CCCH}(44)+\delta_{OCCC}(19)+\tau_{HCCH}(16)$
40	-	-	706	698	7.961	2.342	$\beta_{CCO}(17)+\beta_{CSC}(17)+\beta_{CCC}(13)$
41	-	-	666	659	7.488	1.96	$\beta_{CSC}(31)+\tau_{CCOC}(16)+\beta_{CCO}(15)$
42	654	-	663	656	4.8	1.243	$\tau_{CCOC}(49)$
43	-	-	605	598	4.217	0.911	$\tau_{CCCC}(56)+\tau_{CCCO}(14)+\tau_{CCCB}(14)$
44	594	-	603	596	3.024	0.648	$\tau_{CCCO}(79)$
45	506	-	513	507	5.548	0.861	$\beta_{CCC}(57)+SC(10)$

46	478	-	465	460	5.749	0.735	$\tau\text{CCSC}(48)+\beta\text{CCC}(10)$
47	-	-	450	445	6.679	0.799	$\tau\text{CCSC}(34)+\nu\text{CC}(13)+\beta\text{CCO}(10)$
48	-	-	340	336	3.049	0.208	$\tau\text{CCOC}(52)+\beta\text{CCC}(25)$
49	-	-	333	329	15.32	1.002	$\nu\text{BrC}(53)+\nu\text{SC}(12)$
50	-	-	283	280	9.75	0.461	$\beta\text{CCC}(37)+\beta\text{CCO}(19)+\beta\text{CCBr}(16)$
51	-	-	252	249	5.478	0.205	$\tau\text{CCCC}(42)+\beta\text{CCC}(10)$
52	-	-	221	218	7.023	0.203	$\beta\text{CCC}(29)+\beta\text{CCBr}(15)+\tau\text{CCCC}(15)$
53	-	-	208	205	8.842	0.226	$\beta\text{CCBr}(26)+\beta\text{CCC}(18)+\nu\text{CC}(12)$
54	-	-	172	170	4.961	0.087	$\nu\text{CC}(46)+\beta\text{HCC}(29)+\tau\text{CCCC}(28)+\tau\text{CCBr}(12)$
55	-	-	134	132	7.981	0.085	$\tau\text{CCBr}(38)+\tau\text{CCCC}(36)$
56	-	-	121	119	60878	0.06	$\tau\text{CCCC}(24)+\beta\text{CCC}(21)+\beta\text{CCBr}(11)$
57	-	-	98	97	6.267	0.035	$\tau\text{CCCC}(46)+\tau\text{CCOC}(33)$
58	-	-	46	45	7.677	0.009	$\beta\text{CCC}(46)$
59	-	-	34	33	5.529	0.003	$\tau\text{CCCC}(77)$
60	-	-	12	11	6.487	0	$\tau\text{CCCC}(71)$

The comparable FT-IR and FT-Raman spectra are presented in Figure 2 and Figure 3. Theoretically investigated wavenumbers are usually higher than that of experimental wavenumbers due to the neglect of harmonics in a molecule. Therefore, calculated wavenumbers are scaled down by different scaling factors such as 0.9713 for 4000 to 1700 cm^{-1} and 0.9899 for lower than 1700 cm^{-1} . The calculated vibrational wavenumbers are in line with the experimental wavenumbers after applying the scaling factors.

Figure 2. Experimental FT-IR spectrum of BTF.

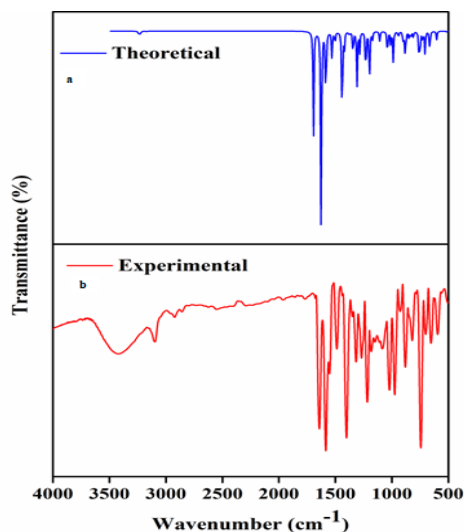
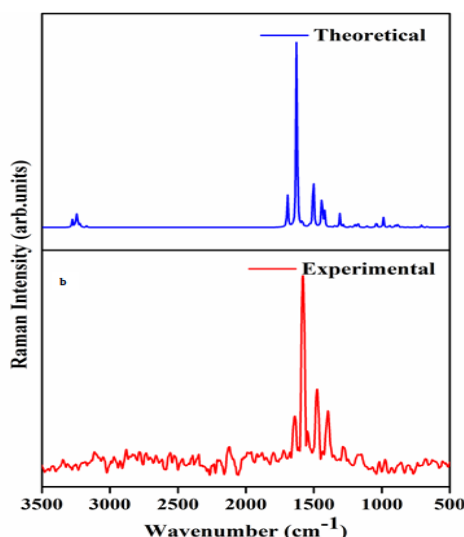


Figure 3. Experimental FT-Raman spectrum of BTF.



C-H vibrations

The organic compounds give rise to the C–H stretching vibrations within the frequency range of 3100– 3000 cm^{-1} [12]. In the present study, the C–H stretching vibration occurs at 3096 cm^{-1} for the FT-IR spectrum and 3047 cm^{-1} for FT- Raman and calculated datas are 3181, 3160, 3150, 3147, 3138, 3125 and 3079 cm^{-1} and PED values acquired at 98, 100, 95, 99, 99, 100 and 99%. The aromatic C–H in plane bending frequencies is sharp with considerable intensity observed within the range from 1300– 1000 cm^{-1} [13]. C–H in plane bending vibrations allocated to 1316, 1268, 1218, 1182 and 1022 cm^{-1} in FT-IR and 1285 and 1019 cm^{-1} in FTRaman spectra and corresponding calculated values are 1362, 1330, 1294, 1271, 1219, 1185, 1100 and 1029 cm^{-1} with PED values of 60, 47, 48, 20, 23, 35, 62 and 66%. The C–H out-of-plane bending modes of BTF appear in the wavenumber range 1000–675 cm^{-1} [14]. Calculated wavenumbers are 999, 888 and 885 cm^{-1} assigned to deformation modes are in accordance with PED values of 93, 36 and 19%.

C-C vibrations

The ring C-C stretching vibrations named skeletal vibration usually appears in the scale between 1400-1625 cm^{-1} [15]. The observed band at 1550, 1487, 1401 and 975 cm^{-1} in FT-IR and 1548, 1476, 1396 and 976 cm^{-1} in FT-Raman spectra and peaks at 1568, 1514, 1487, 1425, 1406, 1330, 1294, 1271, 1219 and 1160 cm^{-1} with the PED values of 62, 74, 54, 75, 31, 13, 12, 35, 11 and 46% calculated by using B3LYP method and these results nearly coincide with the experimental data. Raman band at 860 cm^{-1} and FT-IR at 506 cm^{-1} assigned to a C-C in plane bending mode and theoretical bands exhibit 872, 800, 507, 280 and 218 cm^{-1} with the PED values of 73, 29, 57, 37 and 29% are excellent agreements with the experimental data. The peaks were assigned at 820 and 79 cm^{-1} in FT-IR and FT-Raman to the C-C-C-C deformation mode respectively. The peaks were theoretically determined at 823, 598, 249, 170, 132, 119, 97, 33, and 11 with PED values of 62, 56, 42, 28, 36, 24, 46, 77 and 71%. The predicted BTF values were assigned to the scaled values from the theoretical data.

C=O and C-O vibrations

The vibrational assignments of carbonyl (C=O) group frequencies were observed at strong band owing to the C=O stretching motion of chalcone compounds within the region 1850-1550 cm^{-1} [16,17] and C-O vibration predicted for the area between 1310-1095 cm^{-1} . The frequency of C=O stretching predominantly decided by bond stretch depends upon the inductive, conjugative, and steric effects. C=O stretching frequency was found at 1641 and 1585 cm^{-1} in IR whereas FT-Raman spectrum shows the nearly same frequency at 1640 and 1581 cm^{-1} . Theoretically calculated at 1644 and 1579 cm^{-1} for C=O stretching bands with PED contributions of 38 and 49% respectively. Moreover, the lowering of C=O (carbonyl group) stretching vibration refers to the intramolecular C-H...O hydrogen bonding interactions, which is then assessed by NBO analysis. The C-O is stretching vibrations assigned at 1084 and 926 cm^{-1} for FT-IR spectrum and 1164, 1094 and 933 cm^{-1} calculated theoretically with PED 41, 32 and 51% respectively. The bending vibrations are also observed theoretically within the expected region and it is listed in Table.2

C-S and C-Br vibrations

The stretching vibrations of the C-S were generally difficult to find and are not consistent. The non-polar C-S stretching vibrations were attributed at 975 and 506 cm^{-1} [18] in FT-IR spectrum and 977, 841, 800 and 329 cm^{-1} were observed theoretically with mixed mode using the B3LYP method. The theoretical values are promising with the literature data. The C-S-C is bending modes were calculated at 698 and 659 cm^{-1} and the deformation modes have been observed at 460 and 445 cm^{-1} with the contribution of PED 17, 31, 48, and 34% respectively. The corresponding experimental deformation mode occurs at 478 cm^{-1} in FT- IR spectra. Similarly, the C-Br stretching band was detected at 329 cm^{-1} with a relevant potential energy distribution value of 53%.

Natural Bond Orbital (NBO) analysis

Natural Bond Orbital analysis (NBO) provides extreme insight into the hyper conjugative interactions, inter-intra molecular hydrogen bonding and Electron Density Transfer (EDT) [19]. The second order perturbation theory of the Fock matrix was performed to provide strong information about the stabilization energy $E(2)$ which lies in analyzing the interaction between both occupied Lewis NBO's (bond pair or lone pair) of the donor (i) and an unoccupied Non-Lewis NBO's of the acceptor. Since these interactions lead to loss of occupancy of the localized orbitals of idealized Lewis structure into the anti-bonding orbitals. Thus, to describe the hybridization and delocalization of electron density were determined for the BTF molecule using the DFT method. The corresponding results such as bond orbital and their occupancy (number of electrons), the orbital energy (in atomic unit) and the composition of natural atomic hybrids of the atoms are listed in Table 3. In the NBO analysis, a high $E(2)$ value depicts the intensive interaction between electron donor and electron acceptor that increases the

conjugation of the overall system. Hyper conjugative interactions occur between lone pairs of heteroatoms LP(S5) \rightarrow π^* (C1-C2), LP(O13) \rightarrow σ^* (C4-C8), LP(Br14) \rightarrow π^* (C3-C4), LP(Br14) \rightarrow σ^* (C9-H12) and LP(O17) \rightarrow π^* (C15-C16) having stabilization energies of 28.12, 14.30, 6.82, 13.53 and 22.74 kcal mol⁻¹ respectively. The most effective interaction in the molecule is σ to σ^* transitions. For the title molecule, the intensive hyper-conjugative interaction between σ (C20-H22) to σ^* (C18-H21) leads to the stabilization energy of 85.24 kcal mol⁻¹ and the hyperconjugation between π (C9-C10)to π^* (C8-O13) possess higher stabilization energy of 57.75 kcal mol⁻¹. The other hyper conjugative interactions σ to σ^* from σ (C18-C20) \rightarrow σ^* (C18-H21) and σ (O17-C20) \rightarrow σ^* (C18-H2) produces a stabilization energies of 34.48 and 22.40 kcal mol⁻¹ respectively. The hyper conjugation is related to inter and intra molecular energies leading to the stabilization of a system employing large delocalization.

Table 3. Second order perturbation theory investigations of Fock matrix in NBO basis of BTF compound.

Donor (i)	ED/e	Acceptor (j)	ED/e	aE(j)-E(i)	bE(i,j)	cE(2)
				(a.u)	(a.u)	(kcal mol-1)
LP(S5)	1.549	π^* (C1-C2)	0.326	0.25	0.077	28.12
LP(O13)	1.916	σ^* (C4-C8)	0.07	0.63	0.085	14.3
LP(Br14)	1.939	π^* (C3-C4)	0.419	0.46	0.055	6.82
LP(Br14)	1.934	σ^* (C9-H12)	0.067	0.79	0.092	13.53
LP(O17)	1.708	π^* (C15-C16)	0.297	0.36	0.08	22.74
σ (C1-C2)	1.978	σ^* (C3-Br14)	0.04	0.81	0.064	6.31
π (C1-C2)	1.843	π^* (C3-C4)	0.419	0.43	0.062	9.82
σ (C2-C3)	1.978	σ^* (C4-C8)	0.07	1.08	0.063	4.46
π (C3-C4)	1.82	π^* (C1-C2)	0.014	0.3	0.062	14.91
σ (C4-C5)	1.966	σ^* (C3-Br14)	0.04	0.8	0.07	7.78
σ (C4-C8)	1.971	σ^* (C9-C10)	0.022	1.35	0.068	4.34
σ (C8-C9)	1.966	σ^* (C9-C10)	0.022	1.56	0.103	8.57
σ (C8-O13)	1.987	σ^* (C8-C9)	0.039	1.77	0.088	5.39
π (C8-O13)	1.945	π^* (C2-C10)	0.151	0.73	0.053	4.59
σ (C9-C10)	1.968	σ^* (C8-C9)	0.039	1.59	0.107	8.92
π (C9-C10)	1.733	π^* (C8-O13)	0.344	0.3	0.119	57.75
σ (C9-H12)	1.951	σ^* (C8-O13)	0.022	1.3	0.084	6.71
σ (C10-H11)	1.96	σ^* (C15-O17)	0.041	0.78	0.069	7.64
π (C15-C16)	1.783	π^* (C9-C10)	0.151	0.68	0.059	6.19
σ (C16-C18)	1.965	σ^* (C10-C15)	0.028	1.05	0.08	7.67
σ (O17-C20)	1.988	σ^* (C18-H21)	0.01	5.47	0.313	22.4
σ (C18-C20)	1.987	σ^* (C18-H21)	0.01	5.35	0.384	34.48
π (C18-C20)	1.834	π^* (C15-C16)	0.297	0.3	0.062	14.95
σ (C20-H22)	1.987	σ^* (C18-H21)	0.01	5.17	0.593	85.24

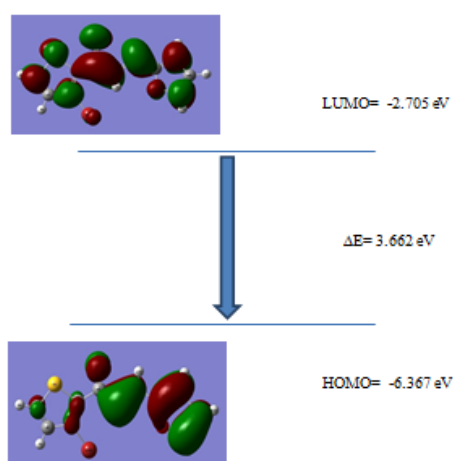
Electronic properties

The frontier molecular orbitals which are the Highest Occupied Molecular Orbital (HOMO) and Lowest Unoccupied Molecular Orbital (LUMO) were examined to understand the chemical reactivity of the molecule. It will be explained by electronic absorption, which is linked to the transition from ground to the first excited state and it is specially denoted by one electron excitation from the HOMO to the LUMO [20,21]. The energies of HOMO and LUMO accurately explicates the global reactivity of the molecule viz., ionization potential ($IP=EHOMO$), electron affinity ($EA=ELUMO$), electronegativity ($\chi=IP+EA/2$), global softness ($S=1/\eta$), global hardness ($\eta=IP-EA/2$) and electrophilicity index ($\omega=\mu^2/2\eta$). The global descriptors are listed in Table 4 and HOMO-LUMO energy plots illustrate in Figure 4.

Table 4. Calculated energy values of BTF B3LYP/6-311+G (d,p) method.

Different parameters	B3LYP/6-311+G(d,p)
E_{HOMO} (eV)	-6.367
E_{LUMO} (eV)	-2.705
Ionization potential (eV)	6.367
Electron affinity (eV)	2.705
Energy gap (eV)	3.662
Electronegativity (eV)	4.536
Chemical potential (eV)	-4.536
Chemical hardness (eV)	1.831
Chemical softness (eV)	0.546
Electrophilicity index (eV)	5.618

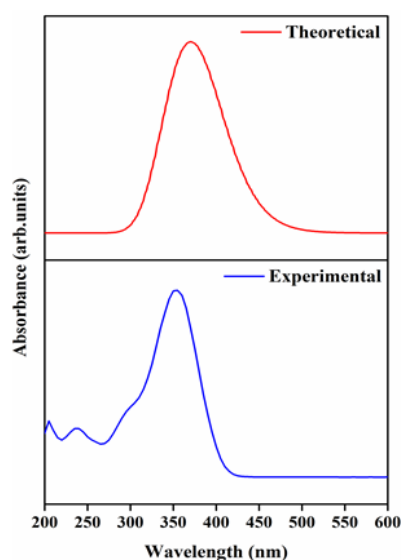
Figure 4. Frontier molecular orbitals, HOMO and LUMO energy gap for the BTF.



HOMO energy lying at -6.3677 eV is localized over the furan ring, C=C and carbonyl (C=O) group whereas LUMO energy is found to be -2.7054 eV which is π^* orbital, localized on the overall compound with large anti-bonding nature. The frontier

orbital energy (ΔE) gap or the HOMO-LUMO gap theoretically obtained is 3.662 eV basis set and the small energy gap of molecule confirms the charge transfer taking place within the molecule. To understand the intramolecular electronic transition of BTF UV-Vis absorption spectra has been studied. The experimental UV-Vis spectrum was recorded at 200- 600 nm using methanol as a solvent. The theoretical UV-Vis spectrum was computed by DFT methods in Figure 5.

Figure 5. Experimental and theoretical UV-Vis absorption spectra of BTF.



The electronic absorption spectra of BTF have experimentally been absorbed in 205, 240 and 355 nm. Theoretically predicted electronic spectra at 355 nm in methanol as a solvent with an oscillator strength $f=0.4154$ which is in agreement with reported values. The maximum absorbed wavelength was assigned from HOMO-3 (highest occupied molecular orbital) to the LUMO (Lowest Unoccupied Molecular Orbital) with 37% contribution. The respective energy band gap was computed for the BTF compound. The UV-Vis spectrum predicts experimentally and theoretically is depicted.

Molecular Electrostatic Potential (MEP)

MEP is a quantitative method utilized to illustrate the electronegativity, structure-activity relationship and relative polarity of the molecule. MEP gives the essential information such as Drug-receptors and enzyme-substrate interactions. The qualitative assessment of MEP is used to predict the electrophilic and nucleophilic reactions to study biological activity and hydrogen bonding interactions (Figure 6) [22,23].

Figure 6. Molecular Electrostatic Potential (MEP) for BTF molecule.

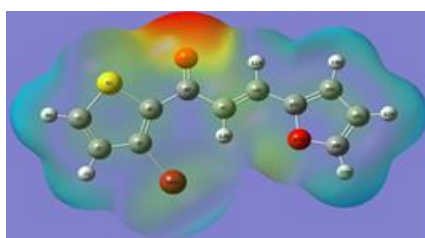


Figure 6 shows a pictorial depiction of the chemical reactivity sites and comparative reactivity of atoms. The most electronegative potential is represented by red color which corresponds to electrophilic reactivity and the most positive electrostatic potential is related to the nucleophilic reactivity which is indicated by blue color. The electrostatic potential is nearly zero for the green region. The negative electrostatic potential was related to an attraction of protons within the molecule (deepest red) whereas positive electrostatic potential was compatible with the repulsion of proton by the atomic nuclei (deepest blue). From the results, the Molecular Electrostatic Potential (MEP) map shows that the electrophilic attack is localized in C=O (carbonyl group) as well as the positive electrostatic potentials was caped on the hydrogen atoms. These are the regions where the molecule can have interactions. The neutral electrostatic potential is localized on the π system of aromatic rings, the most electrophilic site in the oxygen atom for BTF molecule.

Non-Linear Optical properties (NLO)

The non-linear optical properties of the compound have been extensively exploited in telecommunication, signal processing and optical interconnections [24]. The interaction between light and electrons modifies the frequency, phase, or other propagation characteristics, causing NLO effects in organic materials. The strong NLO property is produced by the organic compound which has the large delocalized π -electrons, maximum value of dipole moment and first order hyper polarizability [25]. The dipole moment is considered an essential descriptor because of their measurement of charge movement within the molecule. The whole set of equations utilized for the estimation of magnitude of the total dipole moment (μ), polarizability (α), the anisotropy of polarizability ($\Delta\alpha$) and first order hyper polarizability (β) have been calculated by DFT method and the equations are followed as,

$$\mu_{tot} = (\mu_x^2 + \mu_y^2 + \mu_z^2)^{1/2}$$

$$\alpha = 1/3(\alpha_{xx} + \alpha_{yy} + \alpha_{zz})$$

$$\Delta\alpha = 2^{-1/2} [(\alpha_{xx} - \alpha_{yy})^2 + (\alpha_{yy} - \alpha_{zz})^2 + (\alpha_{zz} - \alpha_{xx})^2 + 6\alpha_{2xx}]^{1/2}$$

$$\beta_{tot} = (\beta_x + \beta_y + \beta_z)$$

$$\beta_x = \beta_{xxx} + \beta_{xyy} + \beta_{xzz}$$

$$\beta_y = \beta_{yyy} + \beta_{xxy} + \beta_{yzz}$$

$$\beta_z = \beta_{zzz} + \beta_{xxz} + \beta_{yyz}$$

These parameters are important for determining the optical properties of the compound. For the BTF compound, the highest dipole moment value ($\mu_{tot} = 2.5463$ Debye) denotes the high electronegativity of the compound, which is also demonstrated by the Molecular Electrostatic Potential (MEP) surface plot. The mean polarizability and first order hyper polarizability of the molecule under exploration is established to be 5.617×10^{-24} esu and 1.171×10^{-30} esu. The result of large polarizability shows that the BTF molecule is biologically active [26], as shown in Table 5. The calculated first order hyper polarizability is 1.171×10^{-30} esu. This is 15.00 times higher than that of urea ($\beta = 7.803 \times 10^{-30}$ esu). Urea is considered a prototypical compound for assessing NLO properties in the molecular system. The results of first order hyper polarizability that confirms the title molecule can be considered as a good NLO active material.

Table 5. The electric dipole moment (μ), polarizability (α) and first hyperpolarizability (β) of investigated compound calculated with B3LYP/6-311+G (d,p).

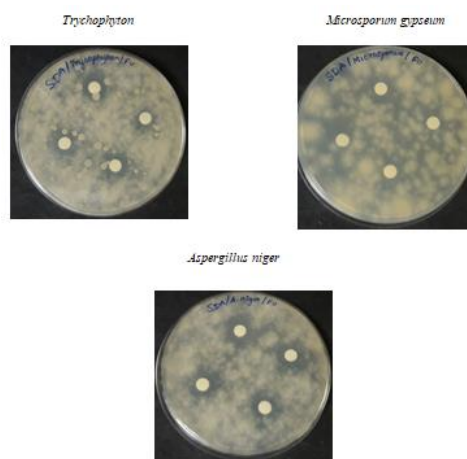
Parameter	DFT/6-311+G(d,p)	Parameter	DFT/6-311+G(d,p)
μ_x	-1.3493	β_{xxx}	-11.0675

μ_y	2.1042	β_{xxy}	14.9432
μ_z	0.4872	β_{xxz}	5.7273
μ_{tot}	2.5463 D	β_{yyy}	98.2419
α_{xx}	-72.30	β_{yyz}	1.5790
α_{yy}	-109.99	β_{xyz}	-9.6431
α_{zz}	-110.43	β_{zzz}	-5.9667
α_{xy}	0.5201	β_{xzz}	13.5624
α_{tot}	5.617×10^{-24} esu	β_{yzz}	21.7453
		β_{xyy}	-13.8672
		β_{tot}	1.171×10^{-30} esu

Antifungal activity

The antifungal activity against BTF compound was studied among three fungi namely *Trichophyton spp*, *Microsporium gypseum* and *Aspergillus niger* compared to the standard Amphotericin-B as displayed in Figure 7.

Figure 7. Antifungal activity of BTF compound.



And the results were presented in Table 6. The zone of inhibition was found to be higher in *Aspergillus niger* (14 mm) when compared to *Trichophyton spp* and *Microsporium gypseum* (10 mm) at the highest concentration of 1000 μ g/mL [27]. That the title compound consists of a more significant inhibitory effect for *Aspergillus niger* from three fungal strains

Table 6. In vitro Antifungal activity of the BTF compound at different concentrations (as MIC in mm).

Zone of inhibition (mm)				
Organisms	Concentration (μ g/mL)			Antibiotic
	1000	750	500	(1mg/mL)

<i>Trychophyton</i>	10	10	9	13
<i>Microsporium gypseum</i>	10	10	9	12
<i>Aspergillus niger</i>	14	13	11	15

Anti-inflammatory activity

Bovine-serum albumin denaturation method was utilized to evaluate the anti-inflammatory property of the BTF Compound. The results were summarized in Table 7.

Table 7. Anti-inflammatory activity of target compound against the serum albumin protein denaturation assay at different concentrations.

Concentration (µg/mL)	Absorbance data at 660 nm	% Inhibition
200	29.28	65.79
400	38.09	74.56
600	43.52	78.76
800	58.59	77.82
1000	75.4	83.85

The activity of the compound was studied with five various concentrations (200, 400, 600, 800 and 1000 µg). All the concentrations showed significant anti-inflammatory activity against bovine serum albumin denaturation; among these, the maximum denaturation activity was observed at the highest concentration (81.83% at 1000 µg/mL) when compared to the control diclofenac sodium [28].

Molecular docking analysis

In this present study, the molecular docking analysis is an explication of the most energetically favourable binding pose of a ligand to its protein in terms of the binding energy. The molecular docking study can be performed by using Auto Dock 4.2.6, which is automated docking software [29]. Originally, the energy of the BTF molecule was minimized by Density Functional Method (DFT). The energy-reduced BTF (ligand) structure was docked at the active site of the 5-LOX (5-lipoxygenase) protein. The binding energy and hydrogen bond value of the drug molecule and their protein targets were completely analyzed for the title compound at where 5-LOX protein interact as represented in Figure 8 (a) and Figure 8 (b) and the values are listed in Table 8.

Figure 8. (a) Ligand interactions of BTF with 5-LOX (5-lipoxygenase).

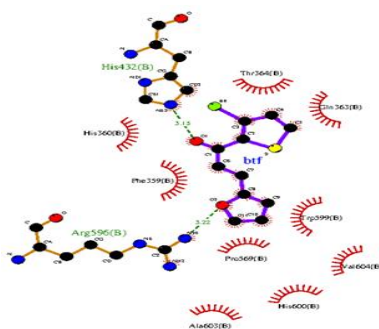


Figure 8. b) Ligand interactions co-crystal of BTF with 5-LOX (5-lipoxygenase).

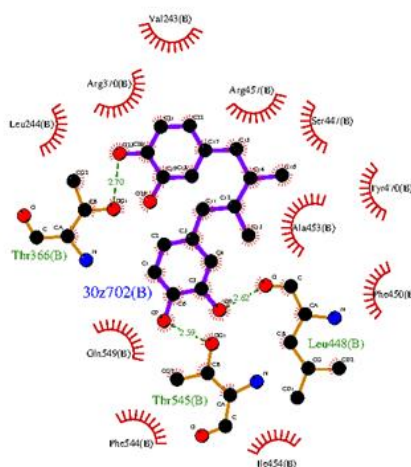


Table 8. Binding energy and ligand interaction hydrogen bond profile of BTF and co-crystal compound with 5-LOX (5-lipoxygenase):PDB ID:6n2w

Compounds	Hydrogen bond interaction	Distance (Å)	Binding energy (kcal/mol)
BTF	His-432	3.15	-5.68
	Arg-596	3.22	
	Thr-366	2.78	
Co-crystal	Thr-545	2.59	-5.35
	Leu-448	2.62	

The 3D crystal structure of the protein was downloaded from the Research Collaborator Structural Bioinformatics (RCSB) protein data bank. Co-crystalline ligand cofactors and all water molecules were removed from the proteins via the Auto Dock Tools (ADT) graphical user interface. Polar hydrogen was later added and atomic charges were calculated using the kollamn and Gasteiger method. The active site of the protein has been defined with grid size 60Å × 60Å × 60Å and the Lamarckian Genetic Algorithm (LGA) has been used to perform the process. A target protein (5-LOX) belongs to a heterogeneous family of cellular responses, associated with normal host defence and inflammation. It catalysis the first two steps in Leukotriene A4

(LTA4) biosynthesis. The oxidation of Arachidonic Acid (AA) at C-5 to yield 5-hydroxy-6,8,10,14-eicosatetraenoic acid (5-HPETE) and the subsequent dehydration to the key intermediate LTA4 (LTA4 synthase activity) which is followed by the synthesis of Leukotrienes (LTS). 5-LOX is implicated in the treatment of various inflammatory diseases such as asthma, allergic and inflammatory disorders [30].

The binding free energy was -5.68 Kcal/mol. The BTF molecule binds with target protein and found to be two hydrogen bond interactions via N-H...O amino acids of His432 at a distance of 3.15 and O-H...N amino acid of Arg-596 at a distance of 3.22 Å. In another case of the co-crystal compound also have three hydrogen bond interactions with active site amino acids of Thr-366, Thr-545 and Leu-448 and distance of 2.78, 2.59 and 2.62 respectively. Based on this results suggest that the title compound could have anti-inflammatory activity. Further, experimental validation is needed for this compound.

CONCLUSION

DFT methods were used to analyze and study the structure, electronic, vibrational and other molecular properties of 2(E)-1-(3-bromothiophene-2-yl)-3-(furan-2-yl)prop-2-en-1-one (BTF). Optimized geometrical parameters (bond lengths and bond angles) are theoretically investigated using the DFT method and compared to the experimental results. The vibrational assignments and PED were examined to confirm the presence of various functional groups. The UV-Visible absorption spectra were recorded for the title compound and also evaluated from the TD-DFT method. The wavelengths of UV absorptions were found to be 205, 240 and 355 nm. The HOMO and LUMO energies were determined and the energy gap was found as 3.662 eV. The electrophilicity (5.618 eV) values were reckoned from the HOMO and LUMO energies and found to be significantly high. This confirms that the BTF as a biologically active. The molecular electrostatic potential shows the electronegative potential on the oxygen atom of a carboxylic group (C=O) while the electropositive potential caped on hydrogen atoms. The predicted first order hyper polarizability of the BTF molecule is 1.171×10^{-30} esu and the dipole moment is 2.546 Debye and the first order hyper polarizability is fifteen times greater than that of NLO standard material urea, which found the BTF molecule to be a good candidate for non-linear optical applications. The antifungal activity results show the greater activity for the *Aspergillus niger* strain as compared to the *Trichophyton* and *Microsporium gypseum* strains. The BTF compound showed good anti-inflammatory activity at 1000 µg/mL with 81.83% when compared to the control diclofenac sodium. From the docking, results reveal that title compound BTF has a good binding ability similar to co-crystal inhibitors.

CONFLICTS OF INTEREST/COMPETING INTERESTS:

The authors declare that they have no conflict of interest.

AVAILABILITY OF DATA AND MATERIAL:

The authors confirm that the data supporting the findings of this study are available within the article

AUTHOR'S CONTRIBUTIONS:

All authors contributed equally to the paper.

REFERENCES

1. Sasi, BA et al. Perspective on quantifying electron localization/delocalization, non-linear optical response and vibrational analysis of 4-(dimethylamino) benzaldehyde-2, 4-dinitroaniline. J Mol Struct. 2017;797-807.
2. Shetty T, et al. Nonlinear absorption, optical limiting behavior and structural study of a new chalcone

- derivative-1-(3, 4-dimethylphenyl)-3-[4 (methylsulfanyl) phenyl] prop-2-en-1-one. Opt Laser Technol. 2016;77:23-30.
- Shetty T, et al. Structural and optical properties of a new organic crystal 3-(2-chloro-5-(trifluoromethyl) phenyl)-1-(3, 4-dimethoxyphenyl) prop-2-en-1-one for nonlinear optical applications. Mater Technol. 2017;32:140-147.
 - Kolev TM, et al. Experimental and computational studies of the structure and vibrational spectra of 4-dimethylamino pyridinium-betaine of squaric acid. J Mol Struct. 2004;691:241-248.
 - Bukhari IH, et al. J Saudi Chem Soc. 2017;21:403-414.
 - Yıldız E, et al. Thiophene based imine compounds: Structural characterization, electrochemical, photophysical and thermal properties. J Mol Struct. 2017;1150:55-60.
 - Ermış E, et al. A new 2, 2'-oxydianiline derivative symmetrical azomethine compound containing thiophene units: Synthesis, spectroscopic characterization (UV-Vis, FTIR, ¹H and ¹³C NMR) and DFT calculations. J Mol Struct. 2018;1168:115-126.
 - Sangeetha P, et al. Electronic properties of solvents (Water, Benzene, Ethanol) using IEFPCM model, spectroscopic exploration with drug likeness and assessment of molecular docking on 1-Octanesulfonic Acid Sodium Salt. J Mol Liq. 2021;344:117-719.
 - Renjith R, et al. Spectroscopic (FT-IR, FT-Raman) investigations and quantum chemical calculations of 1, 7, 8, 9-tetrachloro-10, 10-dimethoxy-4-{3-[4-(3-methoxyphenyl) piperazin-1-yl] propyl}-4-azatricyclo [5.2. 1.02, 6] dec-8-ene-3, 5-dione. Mol Bio. 2021;129:438-450.
 - Vazquez-Vuelvas OF, et al. Crystal structure of the chalcone (E)-3-(furan-2-yl)-1-phenylprop-2-en-1-one. Crystallogr Commun. 2015;71:161-164.
 - Anuradha K, et al. Corrosion inhibition of carbon steel in low chloride media by an aqueous extract of *Hibiscus rosa-sinensis* Linn. Chem Eng Commun. 2017;195:352-366.
 - Liu CH, et al. Human breast tissues studied by IR Fourier-transform Raman spectroscopy. In Conference on lasers and electro-optics (p. CWF51). Optical Society of America.2021.
 - Ramalingam S, et al. Vibrational spectroscopy (FTIR and FTRaman) investigation using ab initio (HF) and DFT (B3LYP and B3PW91) analysis on the structure of 2-amino pyridine. Spectrochim Acta A Mol Biomol. 2010;77:73-81.
 - Ermis E. Synthesis, spectroscopic characterization and DFT calculations of novel Schiff base containing thiophene ring. J Mol Struct. 2018;1156:91-104.
 - Srinivasaraghavan R et al. Molecular conformational stability and Spectroscopic analysis of Parared with experimental techniques and quantum chemical calculations. Spectrochim Acta A Mol Biomol. 2015;137:1194-1205.
 - Sivakumar C, et al. Molecular spectroscopic investigation, quantum chemical, molecular docking and biological evaluation of 2-(4-Chlorophenyl)-1-[3-(4-chlorophenyl)-5-[4-(propan-2-yl) phenyl]-3, 5-dihydro-1H-pyrazole-yl] ethanone. J Mol Struct. 2021;129010.

17. Savithiri S, et al. Synthesis, electronic structure investigation of 3-pentyl-2, 6-di (furan-2-yl) piperidin-4-one by FT-IR, FT-Raman and UV-Visible spectral studies and ab initio/DFT calculations. *Spectrochim Acta A Mol Biomol.* 2015;151:773-784.
18. Potla KM, et al. An analysis of spectroscopic, computational and biological activity studies of L-shaped sulfamoyl benzoic acid derivatives: A third order nonlinear optical material. *J Mol Struct.* 2020;128070.
19. Al-Alshaikh MA et al. Synthesis, vibrational spectroscopic investigations, molecular docking, antibacterial and antimicrobial studies of 5-ethylsulphonyl-2-(p-aminophenyl) benzoxazole. *J Mol Struct.* 2016;1115:94-104.
20. Raja M, et al. Synthesis, spectroscopic (FT-IR, FT-Raman, NMR, UV-Visible), NLO, NBO, HOMO-LUMO, Fukui function and molecular docking study of (E)-1-(5-bromo-2-hydroxybenzylidene) semicarbazide. *J Mol Struct.* 2017;1141:284-298.
21. Kumar R, et al. Molecular structure, spectroscopic (FT-IR, FT Raman, UV, NMR and THz) investigation and hyper polarizability studies of 3-(2-Chloro-6-fluorophenyl)-1-(2-thienyl) prop-2-en-1-one. *J Mol Struct* 2017;1129:292-304.
22. Al-Tamimi AMS, et al. Electronic structure, hydrogen bonding and spectroscopic profile of a new 1, 2, 4-triazole-5 (4H)-thione derivative: A combined experimental and theoretical (DFT) analysis. *J Mol Struct.* 2016;1120:215-227.
23. Kayalvizhi R, et al. Synthesis, characterization, stereochemistry and biological investigation of certain N-dichloroacetyl-bis (2-chlorophenyl) piperidin-4-ones. *J Mol Struct.* 2018;1153:106-118.
24. El-Shoukrofy MS, et al. Pyrazoles containing thiophene, thienopyrimidine and thienotriazolopyrimidine as COX-2 selective inhibitors: Design, synthesis, in vivo anti-inflammatory activity, docking and in silico chemo-informatic studies. *Bio Chem.* 2019;85:541-557.
25. Du L, et al. Binding investigation of human 5-lipoxygenase with its inhibitors by SPR technology correlating with molecular docking simulation. *J biochem.* 2016;4:715-723.
26. Jamalis J et al. Synthesis, spectral characterization (FT-IR, FT-Raman and NMR) and Quantum computational analysis of (E)-1-(4-Bromophenyl)-3-(5-bromothiophen-2-yl) prop-2-en-1-one. *Che Data Coll.* 2020;28:100415.
27. Mathew B, et al. Pharmacophore-based 3D-QSAR analysis of thienyl chalcones as a new class of human MAO-B inhibitors: investigation of combined quantum chemical and molecular dynamics approach. *J Phys Chem B.* 2017;6:1186-1203.
28. Vaazquez RJ, et al. Evaluating the effect of heteroatoms on the photophysical properties of donor-acceptor conjugated polymers based on 2, 6-Di (thiophen-2-yl) benzo [1, 2-b: 4, 5-b'] difuran: two-photon cross-section and ultrafast time-resolved spectroscopy. *J Phys Chem C.* 2017;27:14382-14392.
29. Deghady A M, et al. Density functional theory and molecular docking investigations of the chemical and antibacterial activities for 1-(4-Hydroxyphenyl)-3-phenylprop-2-en-1-one. *Mol.* 2021;26:3631.

30. Junker A, et al. Structure-based design of 3-(4-aryl-1 H-1, 2, 3-triazol-1-yl)-biphenyl derivatives as P2Y₁₄ receptor antagonists. *J Med Chem.* 2016;59:6149-6168.